



HAL
open science

Influence of abrasive grain geometry on friction coefficient and wear rate in belt finishing

Abdeljalil Jourani, Benjamin Hagège, Salima Bouvier, Maxence Bigerelle,
Hassan Zahouani

► To cite this version:

Abdeljalil Jourani, Benjamin Hagège, Salima Bouvier, Maxence Bigerelle, Hassan Zahouani. Influence of abrasive grain geometry on friction coefficient and wear rate in belt finishing. *Tribology International*, 2013, 59, pp.30-37. 10.1016/j.triboint.2012.07.001 . hal-02908780

HAL Id: hal-02908780

<https://hal.science/hal-02908780>

Submitted on 2 Nov 2022

HAL is a multi-disciplinary open access archive for the deposit and dissemination of scientific research documents, whether they are published or not. The documents may come from teaching and research institutions in France or abroad, or from public or private research centers.

L'archive ouverte pluridisciplinaire **HAL**, est destinée au dépôt et à la diffusion de documents scientifiques de niveau recherche, publiés ou non, émanant des établissements d'enseignement et de recherche français ou étrangers, des laboratoires publics ou privés.



Distributed under a Creative Commons Attribution - NonCommercial 4.0 International License

Influence of abrasive grain geometry on friction coefficient and wear rate in belt finishing

A. Jourani ^{a,*}, B. Hagege ^a, S. Bouvier ^a, M. Bigerelle ^{a,b}, H. Zahouani ^c

^a UTC – Centre de recherche Royallieu, Laboratoire de Me´canique Roberval, UTC, UMR 6253, BP20529, 60205 Compi`egne cedex, France

^b Laboratoire Thermique, Energie´tique, Mise en forme, Production, EA 4542, Universite´ de Valenciennes et du Hainaut Cambre´sis, Le Mont Houy, 59313 Valenciennes, France

^c Ecole Centrale de Lyon Laboratoire de Tribologie et Dynamique des Syst`emes, 36 Avenue Guy de Collongue, 69131 Ecully cedex, France

We focus our study on belt finishing process using a 3D model with multi-asperity abrasive wear on real rough surfaces. The established model allows determining the effect of the local geometry of abrasive grain on the friction coefficient and wear rate. This study shows that the friction coefficient and wear rate increase with the local slopes of the roughness. With the increase of the macroscopic normal load, the wear rate increases rapidly. Such effect is related to the increase of the cutting force of each grain leading to the transition in dominant wear mode from ploughing to wedging and cutting.

1. Introduction

Abrasive machining processes are part of the large field of manufacturing processes and include grinding, belt finishing, honing, lapping, polishing, etc. These processes are manufacturing techniques which employ very hard granular particles to modify the shape and surface texture of manufactured parts. In the specific case of the belt finishing process which is considering such as super finishing process, the belt is applied on a rotating workpiece with a defined pressure and an axial oscillation [1–3]. The cutting tool consists in geometrically calibrated abrasive grains of silicon. The micro-geometrical accuracy reached with such process is similar to that obtained using a grinding process. Researches on belt finishing are very limited. The effects of the local geometry of abrasive grains on the local contact parameters such as friction coefficient, wear rate have not yet been fully explained. The understanding of the wear mechanism in belt finishing requires a modelling of the multiple grooving processes during two-body abrasive wear. Several theories have been presented to explain the size effect on the wear rate [4,5]. For small particles, the wear rate increases with increasing particle size. Above some critical size, the wear rate becomes almost

independent of further size increases. This critical size is often about 100 μm . Sin et al. [6] and Suh et al. [7] reported that the size effect was due to the relative bluntness of the abrasive particles. Their theory is based on the observation that, for a given load, blunt shapes produce less wear than sharp one.

Among the models which take into account a multi-asperity abrasive wear [8–9] applied statistical approaches to simulate multiple grooving processes during two-body abrasive wear. In their simulation, the simple classical abrasive wear model was used and pure cutting wear mechanism was assumed. Jiang et al. [10] have proposed an assumption of conical particles with round tips similar to Jacobson's particle model to describe two-body abrasion of metals under multiple contact conditions. In that model, the groove ridge and the particle height distribution are considered. Besides wear mode transitions and material removal fraction under various conditions are also included. The tip radius and apex angle of particles are set as real variables. However, random parameters of particle geometry have not been introduced. Other statistical approaches have been used by [11] in order to evaluate the role of particle distribution and shape in two-body abrasion. Fang et al. [12] used the same approaches to model two-body abrasion process where the particle has a paraboloid of revolution shape. Most approaches presented above consider a multi-asperity abrasive wear to model the contact between the abrasive belt and the metallic surface which is assumed to be smooth. But with these models, it is impossible to obtain the local contact parameters, such as local friction coefficient, tangential forces distribution, or real contact area.

* Corresponding author. Tel.: +33 03 44 23 73 18; fax: +33 03 44 23 44 15.

E-mail addresses: abdeljalil.jourani@utc.fr (A. Jourani), benjamin.hagege@utc.fr (B. Hagege), salima.bouvier@utc.fr (S. Bouvier), maxence.bigerelle@utc.fr (M. Bigerelle), Hassan.Zahouani@ec-lyon.fr (H. Zahouani).

Nomenclature

A_g	Cross-sectional area of the wear groove
A_r	Contact area ratio
A_{r1}, A_{r2}	Quantity of material pushed to the groove sides
a_i^x	Contact radius along x direction
a_i^y	Contact radius along y direction
d20 and d30	Depth displacement using the abrasive paper S20 and S30 respectively
E_j	Young modulus relative to surface j
E^*	Combined Young's modulus of the two surfaces
H	Vickers hardness
F	Total normal load F
f_{ab}	Wear ratio
$F_{c,i}$	Normal force by using the conical model
F_{MAX}	Imposed normal effort
$F_{s,i}$	Normal force by using the spherical model
M	Number of points along x direction
N	Number of points along y direction
n	Total number of summits
P_m	Mean contact pressure

With new improvements of computation capability and commercial software of finite elements method (FEM), three-dimensional FE computations become faster. Buaille et al. [13] and Subhash and Zhang [14], use FEM computation in order to analyse the friction coefficient, the stress and strain fields with a conical indenter-scratching process. They show the existence of a critical attack angle α_c . Below α_c , no material detachment from the wearing surface is observed for α lower than the critical angle α_c . However, increasing the attack angle leads to a transition from micro-ploughing to micro-cutting. It is worth noting that most of the existing FE models, however, mainly deal with single particle contact conditions. In our previous work [1], three-dimensional model was developed by describing the abrasive grains as a distribution of indenters with various attack angles for a local study of a multi-asperity abrasive wear. With this model, the mean pressure and the friction coefficient are constant on each asperity and are independent of the penetration depth. They are only related to the attack angle α of the abrasive grain.

In the present paper, we improve our model by describing the local geometry of the asperity of the abrasive paper as hard conical indenter with a hemispherical tip. The indentation approaches developed for the conical and spherical indenters are coupled and extended to study the abrasive wear mechanisms by considering the three different processes of abrasion. The new developed model is used to determine the effect of particle geometry on the friction coefficient and the material removal rate in the abrasive process at different depths of penetration using three-dimensional real rough surfaces. Conversely to our earlier model, the local contact parameters such as pressure, friction coefficient, and real contact area, wear rate depend in this work, on both the penetration depth and the attack angle of each abrasive grain. A specific application in case of belt finishing process is proposed.

The paper is divided in three main sections. The first one is devoted to the description of the proposed model. The second section is dedicated to the presentation of the numerical implementation of the model and the adopted flowchart. Finally, the third section presents the results in term of friction coefficient, wear rate evolution as a function of the normal load and the size of the abrasive particles. Some concluding remarks and prospects are proposed in the last section of the paper.

Q	Tangential force Q
$Q_{c,i}$	Tangential force using the conical model
$Q_{s,i}$	Tangential force using the spherical model
R_i	Mean radius of the hemispherical tip
Y	Yielding point
z_i	Amplitude at position (x_i, y_i)

Greek letters

α_1	Critical attack angle for ploughing
α_2	Critical attack angle for cutting
α_i	Mean attack angle of abrasive grain
δ_i	Local depth penetration
Δx	Sampling steps along x direction
Δy	Sampling steps along x and y direction
$\Delta z(x_i, y_i)$	The difference of the attitude between two neighbouring points
μ	Mean friction coefficient
ν_j	Poisson's ratio relative to surface j

2. Spherical and conical indentation models

2.1. Spherical geometry of an abrasive grain

The geometry for the contact problem is shown in Fig. 1. Each asperity i is described by a cone with a hemispherical end tip. At a small depths of penetration, *i.e.* the local displacement δ_i , the radius of the hemispherical tip R_i , and the attack angle α_i satisfy the condition $\delta_i \leq R_i(1 - \cos \alpha_i)$ (see Liu et al., [19]), only the spherical tip is in contact.

δ_i corresponds to the depth penetration of the abrasive asperity i into the flat surface. It is computed using the initial position of the flat surface. For each asperity i , this initial position is determined when a first contact is reached between the abrasive grain i and the flat surface. The latter is parallel to the mean plane of the abrasive surface. In the present work, we assume that the abrasive grains do not deform during the belt finishing process.

The Hertz solution [15] for an elastic contact of a sphere and a flat surface provides the mean contact pressure P_m :

$$P_m = \frac{4}{3\pi} E^* \sqrt{\frac{\delta_i}{R_i}} \quad (1)$$

where E^* is the combined Young's modulus of the two surfaces in contact and is given by

$$\frac{1}{E^*} = \frac{1-\nu_1^2}{E_1} + \frac{1-\nu_2^2}{E_2} \quad (2)$$

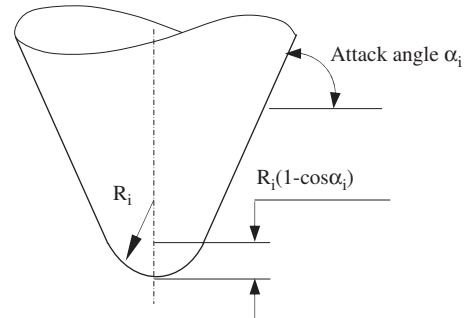


Fig. 1. Geometry of an abrasive grain i .

and E_j and ν_j are respectively the Young modulus and the Poisson's ratio relative to surface j . At the scale of the asperity i , the plastic behaviour begins when the mean contact pressure $P_{m,i}=0.39H$ [16]. For plastically deformed metals, the yielding point Y can be correlated to the Vickers hardness H by $H=3Y$ [16].

The behaviour of the flat surface near the asperity i , may experience three distinct deformation stages as δ_i increases: elastic, elasto-plastic and fully plastic. When δ_i is sufficiently small (i.e. lower than a critical value $\delta_{1,i}$), the material deforms elastically. When δ_i is increased to another critical value $\delta_{2,i}$, fully plastic deformation occurs. When, $\delta_{1,i} < \delta_i < \delta_{2,i}$, the behaviour of the flat surface is elasto-plastic.

The critical penetration depth $\delta_{i,1}$ for the asperity i , can be expressed by [17]:

$$\delta_{i,1} = \left(0.92 \frac{H}{E^*}\right)^2 R_i \quad (3)$$

The deformation is considered entirely plastic ($\delta_i > \delta_{2,i}$) when the contact pressure reaches the hardness of the flat surface material ($P_{m,i}=H$) and the normal contact force F_2 is about 400 times the initial loading F_1 [17]. The latter corresponds to the level of the normal load when the mean pressure reaches the initial yield limit. The corresponding critical displacement δ_2 for a fully plastic deformation is about $\delta_2 \approx 54\delta_1$ (more details are given in [17]). Therefore, from Eq. (3), the following relation is obtained

$$\frac{\delta_{2,i}}{R_i} \approx 45 \left(\frac{H}{E^*}\right)^2. \quad (4)$$

In the specific case of belt finishing, where the abrasive grain sizes are around few unit μm , the critical displacement δ_2 is about $0.075 \mu\text{m}$ (using $H=2100 \text{ MPa}$; $E^*=145 \text{ GPa}$; $R_{\text{mean}} \approx 9 \mu\text{m}$ in Eq. (4)). In the present case the penetration depth of each abrasive grain largely exceeds δ_2 . Therefore, during all the belt finishing process, we consider a perfect plastic contact between the abrasive grain and the work-piece. This assumption remains valid even for low normal loading. The mean pressure P_m is then equal to the hardness H . Using the Tresca criterion [18], the plastic deformation is initiated when the magnitude of the maximum shear stress τ reaches half of the yield stress Y . As $H=3Y$, then $\tau=H/6$.

For spherical contact s of each asperity i whose behaviour is considered to be entirely plastic, the normal force $F_{s,i}$ and the tangential force $Q_{s,i}$ according to [19], can be expressed respectively by:

$$\left\{ \begin{array}{l} F_{s,i} = \frac{\pi}{2} HR_i^2 \left[1 - \left(1 - \frac{\delta_i}{R_i}\right)^2 \right] \\ Q_{s,i} = HR_i^2 \left\{ \cos^{-1} \left(1 - \frac{\delta_i}{R_i}\right) - \left(1 - \frac{\delta_i}{R_i}\right) \left[1 - \left(1 - \frac{\delta_i}{R_i}\right)^2 \right]^{1/2} + 2 \left(\frac{\tau}{H}\right) \left(\frac{\delta_i}{R_i}\right) \right\} \end{array} \right. \quad (5)$$

$F_{s,i}$ and $Q_{s,i}$ will be used in order to determine the friction coefficient at the scale of each abrasive grain.

2.2. Conical geometry of an abrasive grain

At large penetration depth ($\delta_i > R_i(1 - \cos \alpha_i)$), for conical contact c of each asperity i and in case of perfect plastic contact, the normal force $F_{c,i}$ and the tangential force $Q_{c,i}$ acting on the area of the conical surface of the asperity, are given by [19]

$$\left\{ \begin{array}{l} F_{c,i} = \frac{\pi}{2} HR_i^2 \left\{ \left[\left(\frac{\delta_i}{R_i} - 1 + \sec \alpha_i\right) \cot \alpha_i \right]^2 - \sin^2 \alpha_i \right\} \\ Q_{c,i} = HR_i^2 \left[\tan \alpha_i + \left(\frac{\tau}{H}\right) \sec \alpha_i \right] \left\{ \left[\left(\frac{\delta_i}{R_i} - 1 + \sec \alpha_i\right) \cot \alpha_i \right]^2 - \sin^2 \alpha_i \right\} \end{array} \right. \quad (6)$$

Therefore the total normal load F_i and tangential load Q_i acting on the abrasive grain i , is the sum of the force acting on the area of the hemispherical surface and the force acting on the area of the conical surface:

$$\begin{aligned} F_i &= F_{s,i} + F_{c,i} \\ Q_i &= Q_{s,i} + Q_{c,i} \end{aligned} \quad (7)$$

The total normal load F and the tangential force Q supported by the surface are respectively:

$$\left\{ \begin{array}{l} F = \sum_i^n F_i \\ Q = \sum_i^n Q_i \end{array} \right. \quad (8)$$

where n is the number of asperities in contact with the work-piece.

The normal force is primarily responsible for indentation of the grains into the work-piece, whereas the tangential force is responsible for the material removal and overcoming friction. The mean friction coefficient μ , is then given by the ratio between the tangential and the normal forces:

$$\mu = \frac{Q}{F}. \quad (9)$$

3. Flowchart

The model described in the previous section is implemented in Matlab software© to study the contact between an abrasive paper and a smooth plane using the flowchart describes in Fig. 2. The measurement of surface uses the 3-D stylus system. It consists of recording N parallel profiles in a given direction with an acquisition step Δy in an orthogonal direction to that of the profiles. Each profile is discretised with a regular spacing Δx and a number of points M . Therefore the surface topography is characterised by $N \times M$ points. Each point of the coordinates (x,y) has a height z . Data are saved on a disc in the form of binary file and are used as an input in a three dimensional surface topology detection algorithm [20–21]. The latter is used to determine the position and the summit of each asperity. For each summit i located at (k,l) of amplitude $z(k,l)$, the difference $\Delta z(k,l) = z(k,l) - z(s,r)$ is calculated and compared to the heights of the eight neighbouring points. Where $s=k-1, k, k+1$ and $r=l-1, l, l+1$.

If all $\Delta z(k,l) > 0$, $z(k,l)$ will be regarded as the summit of asperity [20–21].

The curvature radius of the summit for each asperity i along the directions x and y ($R_i^x(k,l)$, $R_i^y(k,l)$) with respect to the mean square plane of the surface are defined as

$$R_i^x(k,l) = \frac{180(\Delta x)^2}{2z_{k-3,l} - 27z_{k-2,l} + 270z_{k-1,l} - 490z_{k,l} + 270z_{k+1,l} - 27z_{k+2,l} + 2z_{k+3,l}}, \quad (10)$$

$$R_i^y(k,l) = \frac{180(\Delta y)^2}{2z_{k,l-3} - 27z_{k,l-2} + 270z_{k,l-1} - 490z_{k,l} + 270z_{k,l+1} - 27z_{k,l+2} + 2z_{k,l+3}}, \quad (11)$$

where Δx and Δy are respectively the sampling steps along x and y directions. The mean radius of summit curvature is defined as:

$$R_i = (R_i^x R_i^y)^{1/2} \text{ and } \left\{ \begin{array}{l} R_{\min} = \min_i (R_i) \\ R_{\max} = \max_i (R_i) \\ R_{\text{mean}} = \frac{1}{n} \sum_i R_i \end{array} \right. \quad (12)$$

If the asperity has a conical geometry, the attack angle of the asperity along x and y directions are given respectively by:

$$\tan \alpha_i^x = \frac{\delta_i}{a_i^x}, \quad (13)$$

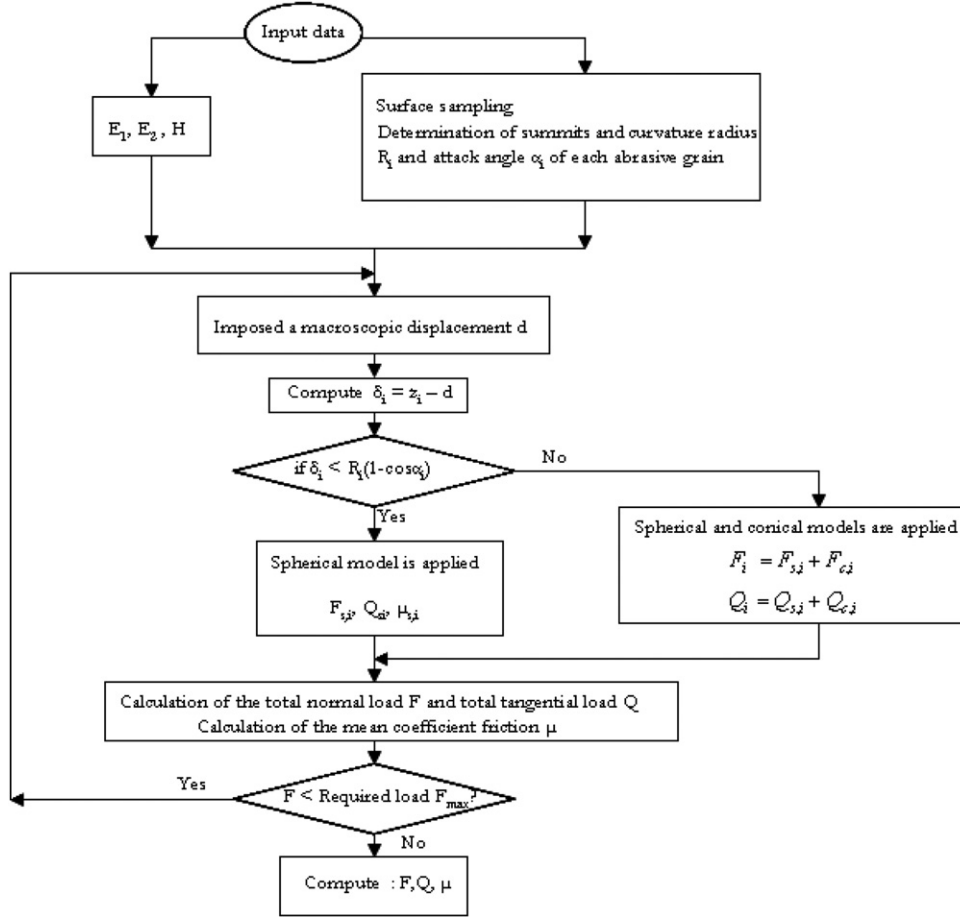


Fig. 2. Flowchart for the numerical prediction of the normal, tangential forces and the local and the macroscopic friction coefficient.

$$\tan \alpha_i^y = \frac{\delta_i}{a_i^y}, \quad (14)$$

where δ_i is the depth penetration of the abrasive grain, a_i^x and a_i^y are the contact radius along x and y directions respectively.

The equivalent attack angle of each asperity is the given by $\alpha_i = \text{mean}(\alpha_i^x, \alpha_i^y)$, $\alpha_{\min} = \min_i(\alpha_i)$, $\alpha_{\max} = \max_i(\alpha_i)$ and $\alpha_{\text{mean}} = 1/n \sum_i \alpha_i$.

The mean radius of summit curvature R_i of asperity increases with the tip radius of the stylus and sampling steps Δx and Δy . However the trend is reversed for the attack angle α_i .

The reproduction of the measured profile is greatly affected by the stylus tip geometry which is defined in terms of the tip radius. The latter is ranging from $2.5 \mu\text{m}$ to $10 \mu\text{m}$. This explains the rounded shape of the abrasive grain.

For a normal macroscopic imposed load F_{MAX} , the two surfaces are progressively put in contact with several increments of displacement Δh of the abrasive paper. Following the value of the critical displacement $R_i(1 - \cos \alpha_i)$, the spherical or conical model can be applied to determine the normal force F_i and the tangential force Q_i . Therefore, the local friction coefficient μ_i is computed at each asperity i (using Eqs. (5) and (6)). Consequently, the total F and Q efforts are generated as well as the global friction coefficient μ . The displacement of the abrasive paper is interrupted when the resulting effort F reaches the imposed normal effort F_{MAX} (i.e. the convergence of the numerical software is reached).

4. Results and discussion

In this work, two abrasive papers are implemented in the model in matrix form with $N \times M$ points. Their corresponding

Table 1
Calculated parameters for the analysed abrasive papers S20 and S30.

	Average grain size (μm)	R_{\min} (μm)	R_{mean} (μm)	R_{\max} (μm)	α_{\min} (rad)	α_{mean} (rad)	α_{\max} (rad)
Surface S20	20	0.58	9.14	52	0.05	0.55	1.34
Surface S30	30	0.3	9.28	60	0.09	0.81	1.42

surfaces are labelled S20 and S30 in the subsequent sections. The average abrasive grain size for S20 and S30 are respectively $20 \mu\text{m}$ and $30 \mu\text{m}$. Three different abrasive papers are taken for each grain size. Besides, the minimum, the maximum and the mean values for the curvature radius of the summits as well as the attack angles for the S20 and S30 surfaces are specified in Table 1 using the relations given in the previous section. These data are indicated in order to simply characterise the examined abrasive surfaces. For the different surfaces, the apparent contact area ($M\Delta x \times N\Delta y$) is $A_{\text{nom}} = 1024 \times 1024 \mu\text{m}^2$ which is discretised using 256×256 points. An example of topography of the two abrasive belts for surfaces S20 and S30 are shown in Fig. 3. The material used for the two abrasive papers is an aluminium oxide Al_2O_3 ($E_1 = 350 \text{ GPa}$; $\nu_1 = 0.25$, $H_0 = 11.75 \text{ GPa}$). The smooth plane is a standard carbon steel AISI 1046 ($E_2 = 210 \text{ GPa}$; $\nu_2 = 0.3$; $H = 2100 \text{ MPa}$). The elastic constants are used in order to compute the equivalent modulus (see Eq. (2)). H is used in order to determine the attack angles α_1 and α_2 that characterise the different wear mechanisms, according to Fig. 9.

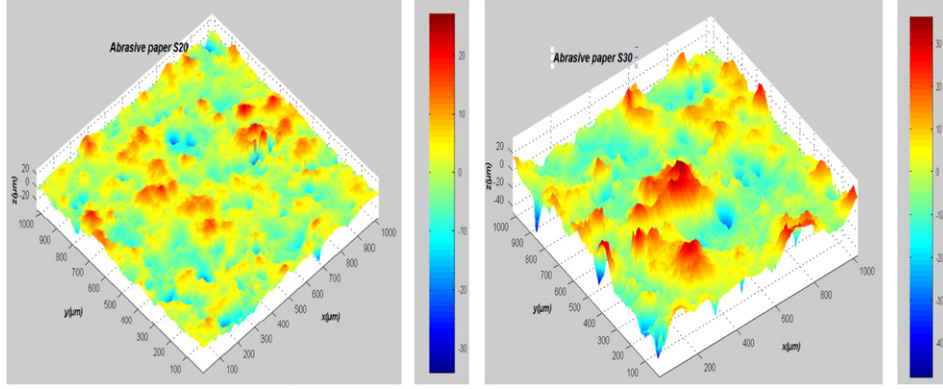


Fig. 3. Topographies of the two abrasive papers S20 and S30 ($1024 \times 1024 \mu\text{m}^2$ which contains 256×256 points). Abrasive paper with an average grain size of $20 \mu\text{m}$ (figure on the left) and $30 \mu\text{m}$ (figure on the right).

Results for S20 and S30 are the average of data obtained with the three different surfaces. The error bars are added in figures at ± 1 standard deviation.

4.1. Effect of the local geometry of the abrasive grains on the tangential load and friction coefficient

Fig. 4 shows the evolution of the macroscopic tangential force Q as function of the normal load F (Eq. (8)) for the surfaces S20 and S30. At small loads ($F < 1.25 \text{ N}$), the tangential force does not evolve linearly as a function of the normal load. The spherical part of each abrasive grain in contact seems to be responsible for such nonlinear behaviour at the beginning of Q vs. F curve. Indeed, the normal and the tangential loads depend on depth penetration. When the influence of the conical part of the tip is dominant, the friction force tends to evolve linearly as a function of the normal force because for the conical tip, the normal and the tangential loads depend only on the attack angle and not on the penetration depth as for the spherical model. Similar trends are observed for the two surfaces. However, as can be expected, the tangential load for S30 is higher than S20. This difference is due to the average attack angle which is more important for S30.

Fig. 5 shows the mean friction coefficient as a function of the macroscopic normal load F . At the early stage of loading, the friction coefficient increases rapidly, because the contact is supported mainly by the spherical part of the abrasive grains. As the mean curvature radius for S20 and S30 surfaces are almost identical (Table 1), the normal and tangential forces F and Q (Eq. (8)) for S20 and S30 coincide for small depth penetration because they only depend on the curvature radius, displacement and hardness of the soft material. In the present model, the interactions between asperities are not taken into account. Consequently, similar friction coefficients are obtained for both abrasive papers. For more important depths, both spherical and conical geometries are combined and affect the friction coefficient evolution. Therefore, the gap between the friction coefficients for surfaces (S20) and (S30) increases with the applied normal load. For very larger depths (*i.e.* higher normal load), the friction coefficient becomes almost constant as observed in Fig. 5. Indeed, the abrasive grains behave as perfect cone indenters where the friction coefficient depends only on the attack angles. The effect of the spherical part of the abrasive particles becomes negligible. The difference between $\mu(\text{S20})$ and $\mu(\text{S30})$ becomes constant and as expected, the friction coefficient $\mu(\text{S30})$ is higher than $\mu(\text{S20})$. This difference is due primarily to the mean attack angles which are more important for the abrasive paper S30.

The evolution of the friction coefficient during the belt finishing process has been studied experimentally by [22] using the

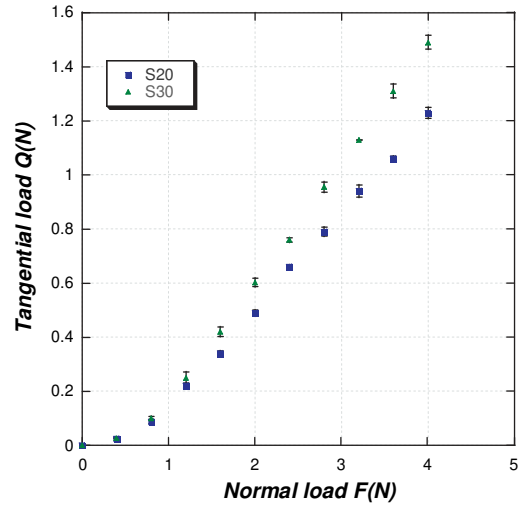


Fig. 4. The evolution of the macroscopic tangential force Q vs. the macroscopic normal force F .

same paper S30 on rough surface, where $R_a = 0.15 \mu\text{m}$. The Fig. 6 shows the comparison between the numerical and experimental friction coefficients as function of the apparent contact pressure (*i.e.* the normal load divided by the apparent contact area). Note that in the present work, for the sake of simplicity, the counterpart is modelled as a perfect smooth surface (*e.g.* standard carbon steel AISI 1046 as indicated in Section 4). This assumption is motivated by the fact that abrasive paper has a relatively high roughness (*e.g.* $R_a \approx 9.4 \mu\text{m}$ for S30) compared to the abraded surface. It can be seen that the two curves have the same trend and increase as the apparent contact pressure increases. The roughness is described by the distribution of the asperity heights. The number of asperities in contact increases with the normal load. This increases the experimental and numerical friction coefficients. The asperities which are not in contact do not contribute in the evaluation of the friction coefficient. However, the experimental friction coefficient is slightly larger than the calculated one. This gap is probably caused by the absence of the adhesive component in the model. The difference between the model and the experiment decreases with the force because the friction coefficient related to the adhesion decreases with increasing normal load.

The evolution of the contact area ratio A_r (*i.e.* real to apparent contact area ratio) with the total normal load is important for understanding the mechanisms involved in friction, adhesion, or wear. Fig. 7 presents the evolution of A_r as a function of the total

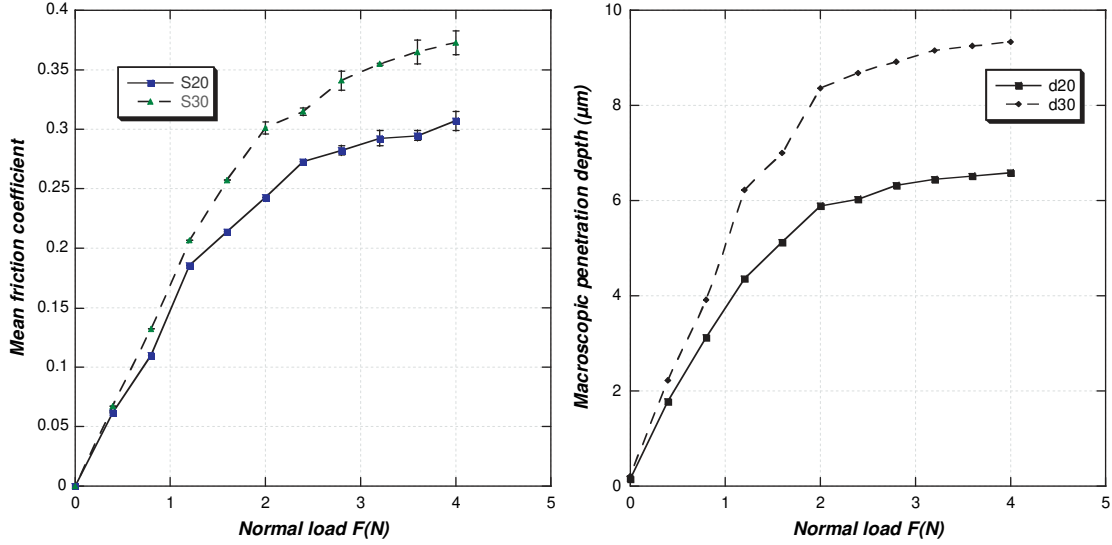


Fig. 5. Mean friction coefficient $\mu(S20)$ and $\mu(S30)$ (figure on the left) and macroscopic penetration depth $d20$ and $d30$ (figure on the right) as function of the macroscopic normal load F for abrasive papers S20 and S30 respectively.

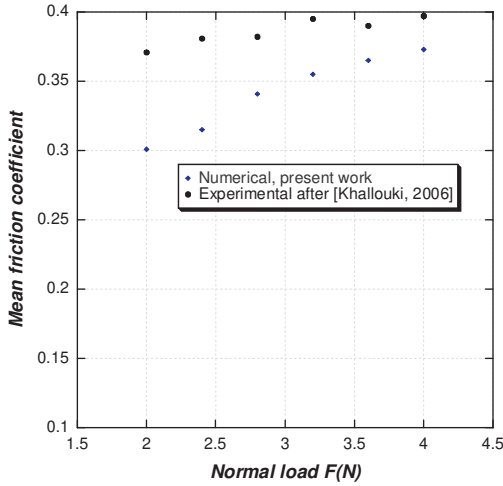


Fig. 6. Comparison between numerical and experimental friction coefficients as a function of the apparent contact pressure.

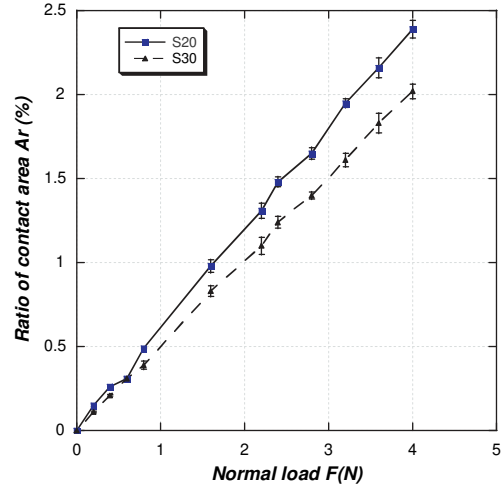


Fig. 7. Evolution of the ratio of contact area vs. the total normal load.

normal load F for both surfaces S20 and S30. The simulations show that A_r is linearly proportional to the normal load which is in agreement with the models developed by [23–24]. It is worth noting that the real contact area between the abrasive paper and the work-piece is much smaller than the apparent one and does not exceed 2.5% of the apparent contact area for the tested abrasive papers.

Fig. 7 indicates also that the contact surface is smaller with paper S30; consequently the corresponding friction coefficient should be smaller than for the abrasive paper S20. A small area of real contact involves a weak adhesion between the abrasive paper and the smooth surface [25]. This is the case for the belt finishing where the adhesion friction coefficient does not exceed 0.05 [22,26]. The value of the friction coefficient is mainly dependent of the local geometry of the abrasive grain via the curvature radius and the attack angle.

4.2. Effect of the local geometry of the abrasive grains on the wear rate

The local contact parameters (e.g. the normal and tangential forces at the asperity scale) are used to determine the material removal during the polishing process and to understand the

effects of the local geometry of the abrasive grains and the apparent contact pressure on wear rate evolution. The abrasive wear can be expressed through three different processes: ploughing, wedge formation, or cutting. The transition from one to another depends on the attack angle α_i of the abrasive grain i computed as in the previous section from the ratio between the groove depth δ and the half-width of the groove a . The influence of the attack angle on the scratch testing of aluminium alloy sample was studied experimentally by [27] by using a single point scratch. Based on their experiments, they have shown that when the attack angle is below 0.51 rad, a ploughing mechanism occurs, whereas for an attack angle above 1.02 rad, a cutting mechanism dominates. For intermediate attack angles a transition from ploughing to cutting wear mechanism has been observed.

The cross section area of the groove produced by each abrasive grain i at a depth δ_i is equal to A_i from which a fraction is removed to cause direct material loss during material displacement in the abrasive process. Such fraction is estimated with the wear ratio f_{ab} [28] and is equals to

$$f_{ab} = \frac{A_g - (A_{r1} + A_{r2})}{A_g}, \quad (15)$$

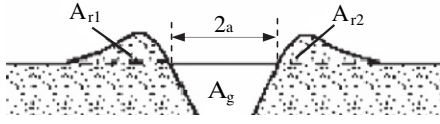


Fig. 8. The cross-sectional profile of the wear groove.

where the different sections are given in Fig. 8. $(A_{r1}+A_{r2})$ represents the quantity of material which is pushed to the groove sides due to the plastic deformation and A_g is the cross-sectional area of the wear groove.

Refs. [29] and [30] have shown that the wear ratio f_{ab} itself depends on the attack angle α of the grains. The latter is defined by

$$\operatorname{tg} \alpha = \frac{\delta}{a}. \quad (16)$$

f_{ab} value becomes equal to zero for ideal microploughing when the attack angle is below some critical value α_1 and equal to unity for ideal microcutting when the attack angle is above some critical attack angle α_2 . Between α_1 and α_2 , the two mechanisms cutting and ploughing coexist simultaneously. In this case $0 < f_{ab} < 1$ and f_{ab} is given by [10]

$$f_{ab}(\alpha) = \frac{\tan \alpha - \tan \alpha_1}{\tan \alpha_2 - \tan \alpha_1} \quad (\alpha_1 < \alpha < \alpha_2). \quad (17)$$

To determine the two critical attack angles α_1 and α_2 , the experimental measurement of Hokkirigawa et al. [30–31] are used (Fig. 9). The authors applied several conical indenters with different attack angles during the scratch test in order to investigate the different wear mechanisms. Such tests are used as a method of constructing a wear mode diagram for different scratched surfaces displaying various Vickers hardness HV. The boundaries conditions between various abrasive wear mechanisms can then be defined in terms of critical attack angles. In our case, where $HV=210$ (measured in the hardness Vickers scale HV30), the two critical angles are $\alpha_1=0.43$ rad and $\alpha_2=0.96$ rad.

At small depth of penetration ($\delta_i \leq R_i(1 - \cos \alpha_i)$), the cross section area of the groove produced by each abrasive grain (i.e. the scratched section) can be calculated by [19]:

$$A_s = \frac{1}{2} R^2 \left\{ 2 \cos^{-1} \left(1 - \frac{\delta}{R} \right) - \sin \left[2 \cos^{-1} \left(1 - \frac{\delta}{R} \right) \right] \right\}. \quad (18)$$

The previous relation is applied at each asperity i . For simplicity, the indices i are omitted in Eqs. (18) and (19). At large penetration depth ($\delta_i > R_i(1 - \cos \alpha_i)$), the cross section area of the groove produced by each abrasive grains is given by [19]:

$$A_c = \frac{R^2}{2 \sin \alpha} \left[2 \alpha \sin \alpha + 2 \frac{\delta}{R} - 2 + 3 \cos \alpha - \cos^3 \alpha + \left(\frac{\delta}{R} \right)^2 \cos \alpha - 2 \frac{\delta}{R} \cos \alpha - \sin \alpha \sin 2 \alpha \right]. \quad (19)$$

In this section, the same abrasive papers S20 and S30 used previously are utilised to study the effect of the abrasive grains size on the wear volume by considering the three different processes of abrasion: ploughing, wedge formation and cutting. The different abrasion mechanisms at the scale of each asperity occur, depending on the value of the attack angle α_i and the two critical attack angles α_1 and α_2 . Table 2 shows the percentage of each wear mechanism for the two abrasive papers S20 and S30.

Fig. 10 shows that the wear volume per unit sliding distance L increases with the total normal load for the two abrasive papers. At low load, the wear volume increases slowly because a large fraction of the total load is carried by a ploughing contact (nonwear contact) and the contact is established mainly by the spherical tip of the asperities which cause plastic deformation as indicated in Section 2.1 without resulting in material removal.

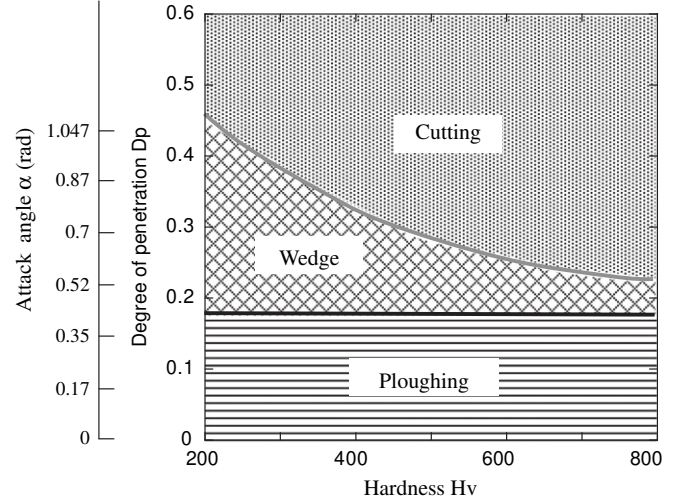


Fig. 9. Wear mode diagram [30,31].

Table 2

Percentages of each wear mechanism for the two abrasive papers S20 and S30.

	Density (%) ($\alpha \leq \alpha_1$)	Density (%) ($\alpha_1 < \alpha < \alpha_2$)	Density (%) ($\alpha_2 < \alpha$)	α_{min} (rad)	α_{mean} (rad)	α_{max} (rad)
Surface S20	43	37	20	0.05	0.55	1.34
Surface S30	31	35	34	0.09	0.81	1.42

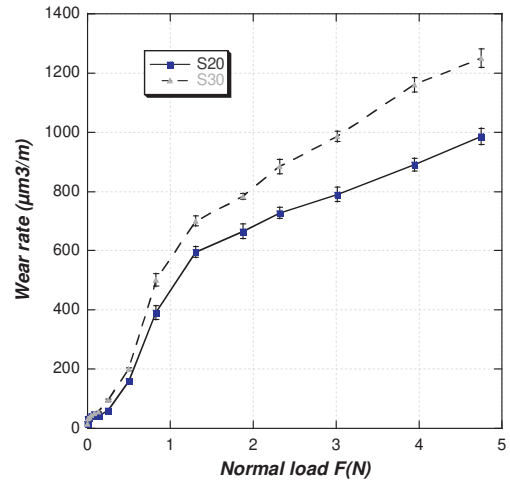


Fig. 10. Wear volume per unit sliding distance L as a function of the normal load for papers S20 and S30.

With the increase in the total normal load, the effect of the spherical part of an individual abrasive grain becomes less significant. The wear rate increases rapidly due to the increase of the cutting force of each grain leading to the transition in dominant wear mode from ploughing to wedging and cutting. The dependence of the groove cross-section area ($A_{r1} + A_{r2}$) increases with the increase of the penetration depth.

With the abrasive paper S30, the general trends for the variation of the wear rate with the applied normal load are similar to the paper S20. However, as can be expected, wear rates are higher compared to the first case. This difference is due primarily to the average attack angle which is more important for S30 where 69% of asperities have attack angles exceeding α_1 . With the increase in the attack angle, the local load supported by an individual grain

increases, leading to the transition in the dominant wear mechanism from ploughing to wedging and cutting.

Table 2 shows also that 43% of abrasive grains of S20 and 31% of S30 do not participate directly to the wear process. Indeed, parts of such grains may only deform plastically without resulting in direct material removal. However, since they change the surface roughness, they may affect the wear process induced by the other grains.

5. Conclusion

During abrasion machining, the effect of the local geometry of the abrasive grains is very important on the local contact parameters as the local friction coefficient, the temperature distribution, the material removal rate. To determine these contact parameters, we established a three-dimensional model by describing the abrasive grains as a distribution of indenters with various attack angles. The local geometry of each asperity is considered as conical with hemispherical tip. Conical and spherical models are combined to determine the normal and the tangential loads as well as the friction coefficient on each abrasive grain and therefore the mean friction coefficient and the wear rate evolution. The belt finishing process of a carbon steel smooth surface with two alumina abrasive papers of different grit sizes is analysed. The numerical results show that:

- Overall, nonlinear evolution of the tangential force as function of the normal load is observed. A parabolic regime is present at small loads. This variation is explained by the fact that the geometry of the abrasive grains has a rounded shape due to the effect of the stylus tip geometry used in the measurement technique. In this case, the local coefficient of friction and the material removal rate depend on the penetration depth. For higher depths, both the spherical and the conical geometries are combined to model the contact between the abrasive grains and the workpiece. At large penetration, the effect of the hemispherical tip is secondary, and the conical geometry becomes dominant.
- The experimental friction coefficient for the same material is slightly larger than the calculated friction coefficient in the present work. This difference is probably caused by the absence of the adhesive component in the model. The simplified geometry used to describe the shape of the abrasive grain (*i.e.* hard conical indenter with hemispherical tip) may also explain the difference between the experimental and numerical results.
- The use of two abrasive papers S20 and S30 shows that the friction coefficient and the wear volume increase with the increase of the abrasive grains size and consequently with the average attack angle of the asperities. Indeed, in such situation, the local load supported by the individual grains increases, leading to the transition in the dominant wear mechanism from ploughing to wedging and cutting.

References

- [1] Jourani A, Dursapt M, Hamdi H, Rech J, Zahouani H. Effect of the belt grinding on the surface texture: modeling of the contact and abrasive wear. *Wear* 2005;259:1137–43.
- [2] Rech J, Kermouche G, Grzesik W, García-Rosales C, Khellouki K, García-Navas V. Characterization and modelling of the residual stresses induced by belt

- finishing on a AISI52100 hardened steel. *Journal of Materials Processing Technology* 2008;208:187–95.
- [3] Bigerelle M, Hagege B, El Mansori M. Mechanical modelling of micro-scale abrasion in superfinish belt grinding. *Tribology International* 2008;41(11):992–1001.
- [4] Backer WR, Marshall FR, Shaw MC. The size effect in metal cutting. *Transactions of the American Society of Mechanical Engineers* 1952;74:61–71.
- [5] Larsen-Basse J. Influence of grit size on the groove formation during sliding abrasion. *Wear* 1968;11:213–22.
- [6] Sin H, Saka N, Suh NP. Abrasive wear mechanisms and the grit size effect. *Wear* 1979;55:163–90.
- [7] Suh NP, Sin HC, Saka N. Fundamental aspects of abrasive wear. In: Such NP, Saka N, editors. *Fundamentals of Tribology*. Cambridge: MIT Press; 1978. p. 493–518.
- [8] Jacobson S, Wallén P, Hogmark S. Correlation between groove size, wear rate and topography of abraded surfaces. *Wear* 1987;115:83–93.
- [9] Jacobson S, Wallén P, Hogmark S. Fundamental aspects of abrasive wear studied by a new numerical simulation model. *Wear* 1988;123:207–23.
- [10] Jiang J, Sheng F, Ren F. Modelling of two-body abrasive wear under multiple contact conditions. *Wear* 1998;217:35–45.
- [11] De Pellegrin DV, Stachowiak GW. Evaluating the role of particle distribution and shape in two-body abrasion by statistical simulation. *Tribology International* 2004;37:255–70.
- [12] Fang L, Li B, Zhao J, Sun K. Computer simulation of the two-body abrasion process modeling the particle as a paraboloid of revolution. *Journal of Materials Processing Technology* 2009;209:6124–33.
- [13] Bucaille JL, Felder E, Hochstetter G. Mechanical analysis of the scratch test on elastic and perfectly plastic materials with the three-dimensional finite element modelling. *Wear* 2001;249:422–32.
- [14] Subhash G, Zhang W. Investigation of the overall friction coefficient in single-pass scratch test. *Wear* 2002;252:123–34.
- [15] Hertz H. On the elastic contact of elastic solids. *Journal für die Reine und Angewandte Mathematik* 1881;92:156–71.
- [16] Tabor D. *The Hardness of Metals*. Oxford University Press; 1951.
- [17] Zhao Y, Maietta D, Chang L. An asperity microcontact model incorporating the transition from elastic deformation to fully plastic flow. *Journal of Tribology* 2000;122(1):86–93.
- [18] Hill R. *The Mathematical Theory of Plasticity*. London: Oxford University Press; 1950.
- [19] Liu Z, Sun J, Shen W. Study of plowing and friction at the surfaces of plastic deformed metals. *Tribology International* 2002;35:511–22.
- [20] Jourani A. Etude expérimentale et modélisation du contact rugueux. PhD thesis. Ecole Centrale, Lyon, France; 2005.
- [21] Zahouani H, Vargiolu R, Loubet JL. Fractal models of surface topography and contact mechanics. *Mathematical and Computer Modeling* 1998;28:517–34.
- [22] Khellouki A. Caractérisation des mécanismes de coupe en superfinish par toilage et de l'intégrité de surface induite dans le cas des aciers traités. PhD thesis. École Nationale Supérieure des Mines, St-Étienne, France; 2006.
- [23] Abbott EJ, Firestone FA. Specifying surface quality—a method based on accurate measurement and comparison. *Mechanical Engineering* 1933;55:569–72.
- [24] Pullen J, Williamson JBP. On the plastic contact of rough surfaces. *Proceedings of the Royal Society A* 1972;327:159–73.
- [25] Takadoum J. *Materials and Surface Engineering in Tribology*. Besançon: Wiley; 2008.
- [26] Puthanangady TK, Malkin S. Experimental investigation of the superfinishing process. *Wear* 1995;185:173–82.
- [27] Mezlini S, Kapsa Ph, Henon C, Guillemet J. Abrasion of aluminium alloy: effect of subsurface hardness and scratch interaction simulation. *Wear* 2004;257:892–900.
- [28] Childs THC. Microstructure and wear of materials. *Wear* 1988;126(1):111–2.
- [29] Goddard HJ, Harker H. A theory of the abrasion of solids such as metals. *Nature* 1959;184:333–5.
- [30] Hokkirigawa K, Kato K, Li Z. The effect of hardness on the transition of the abrasive wear mechanism of steels. *Wear* 1988;123:241–51.
- [31] Hokkirigawa K, Kato K. An experimental and theoretical investigation of ploughing, cutting and wedge formation during abrasive wear. *Tribology International* 1988;21:51–7.